1989-10

Barotropic Vortex Stability to Perturbations from Axisymmetry

Carr, L.E. III; Williams, R.T.

Carr III, L. E., and R. T. Williams. "Barotropic vortex stability to perturbations from axisymmetry." Journal of the Atmospheric Sciences 46.20 (1989): 3177-3191.
https://hdl.handle.net/10945/62200

Barotropic Vortex Stability to Perturbations from Axisymmetry

L. E. CARR III AND R. T. WILLIAMS

Department of Meteorology, Naval Postgraduate School, Monterey, California

(Manuscript received 1 December 1988, in final form 30 May 1989)

ABSTRACT

Tropical cyclones and dynamically similar model vortices robustly maintain a near-axisymmetric horizontal structure where the vortex flow is strongly nonlinear in spite of persistent asymmetric forcing represented by horizontal variations in the environmental winds and the Coriolis parameter. Since tropical cyclone motion relative to environmental "steering" has been associated with vortex asymmetries in even the simplest numerical models, identification of a barotropic mechanism that stabilizes vortices to dispersive influences is important.

A nondivergent, barotropic analytical model is used to identify the asymmetry-damping influence of symmetric angular windshear as the mechanism by which a barotropic vortex resists asymmetric forcing. Solutions are obtained for the evolution of linear asymmetric perturbations imposed as initial conditions on a steady, Rankine vortical flow. Perturbations combining various radial and azimuthal structures that might be expected from environmental and convective forcing are shown to damp with time in an algebraic "continuous spectrum" manner similar to perturbations imposed on f-plane barotropic Couette flow. Closed-form solutions to the model are used to explain why the damping rate is proportional to perturbation azimuthal wavenumber and the local magnitude of the symmetric angular windshear. The damping process is formally shown to be a barotropically stable energy transfer from perturbation to symmetric vortex, and independent numerical evidence is presented to verify the accuracy of the model. The energy transfer process is used to explain barotropic vortex adjustment to changes in external forcing, particularly the initial adjustment phase of a symmetric vortex in response to steady asymmetric forcing that has been documented in various numerical simulations of tropical cyclone motion.

1. Introduction

Many investigations of environmental influences on tropical cyclone (TC) motion, have been conducted using a variety of dynamical models. These studies have shown that the presence of vorticity gradients (planetary and environmental) and any associated horizontal windshear will introduce asymmetries into an initially symmetric vortex scaled to approximate a TC. Although these asymmetries are relatively small, they can cause the motion of the vortex center to be different from that expected due to simple environmental "steering." Early examples of nondivergent, barotropic (NDBT) studies are Adem (1956) concerning the influence of the earth's rotation as approximated by a β-plane (now commonly called the "β-effect") and Kasahara (1957), who also noted the effect of linear environmental windshear. By the 1970s, divergent barotropic (Anthes and Hoke 1975) and baroclinic (Madala and Piascek 1975) numerical modeling studies of TC motion were providing increasing evidence that vortex asymmetries due to the β-effect tended toward a quasi-steady amplitude over the more intense region of the vortex, as manifested by an approximately steady 2–3 m s^{-1} translation of the vortex in a quiescent environment. A later NDBT study by DeMaria (1985; hereafter referred to as DM) included steady, but spatially variable environmental winds, and again noted an approximately steady translation of the vortex after an initial 24 h adjustment period. By subtracting the symmetric vortex from the output of a NDBT numerical model, Fiorino and Elsberry (1989; hereafter referred to as FE) have explicitly demonstrated the quasi-steady nature of a β-induced asymmetry in a TC vortex. Quasi-geostrophic (McWilliams and Flierl 1979) and primitive equation (Mied and Lindemann 1979) model vortices scaled to approximate ocean eddies have also been noted to translate while resisting β-induced dispersion in a manner similar to the TC models. Since horizontal variability of the environment (including β) represents persistent asymmetric forcing with respect to an embedded vortex, it is significant that the response of these model vortices to such forcing is one of minor, quasi-steady deformation and slow dispersion, rather than one of steadily increasing deformation and rapid dispersion.

Observations of TC and ocean eddy persistence are consistent with the results of the simple models. Gulf Stream cold-core rings have been observed to persist for over a year (Cheney and Richardson 1976) while moving through the horizontally sheared Gulf Stream

Corresponding author address: LCDR L. E. Carr III, Dept. of Meteorology, Code 63, Naval Postgraduate School, Monterey, CA 93943-5000.

recirculation region. These rings are often highly elliptical immediately after being formed from pinched-off Gulf Stream meanders, but generally regain a near circular shape within 2 weeks (McCalpin 1987). Tropical cyclones typically persist at or greater than tropical storm strength (>34 kt; 17 m s^{-1}) for 4–6 days, and usually dissipate due to the loss of a low-level source of warm, moist air as they travel north or make landfall, rather than by being destroyed by dynamical dispersion. For example, Typhoon Wayne (1987) persisted at or near typhoon strength (>64 kt; 32 m s^{-1}) for 20 days while embedded in the strongly sheared environment of the monsoon trough (JTWC 1987).

Thus, both modeling and observation evidence suggests that some mechanism(s) inherent to these atmospheric and oceanic vortices renders them highly resistant to Rossby wave dispersion due to large-scale vorticity gradients and deformation due to horizontal shear in the environment. Although it might be argued that the strong thermodynamic forcing that maintains a TC would also promote horizontal axisymmetry, the generally asymmetric distribution of convection in the vicinity of the eyewall actually represents additional asymmetric forcing that should distort the inner windfield. Thus, the prolonged persistance of ocean eddies in a near-symmetric state without thermodynamic forcing and the asymmetry-inducing influence of such forcing in TCs, suggests that the dispersion-resistant properties of these vortices must have a dynamical basis.

It is known that nonlinear advection is necessary to permit dispersion-resistant movement of model vortices in general (e.g., McWilliams and Flierl 1979; Chan and Williams 1987), or nondispersive movement in the case of very specialized entities known as either modons or solitary eddy solutions (see Flierl et al. 1980); however, the precise mechanism by which nonlinear advection stabilizes a vortex of arbitrary radial structure has not been identified. Although Holland (1983) has suggested that inertial stability accounts for near axisymmetry in the inner 300 km of a TC, inertial stabilization cannot occur in the NDBT and quasi-geostrophic models cited above. Thus, the mechanism that accounts for vortex stability must be fundamentally a vorticity advection process, perhaps modified to some extent by more complex processes.

The purpose of this paper is to identify this hypothetical vorticity advection stability mechanism using a NDBT analytical model that includes the asymmetry-inducing influence of β and environmental windshear. Thus, the dynamical situation will be equivalent to DM. Since a complete solution (transients and quasi-steady-state) to that model is in all likelihood analytically insolvable, this paper will address primarily the transient adjustment process toward the quasi-steady-state by transforming the forced problem into the related unforced initial value problem. The model is developed and solved in section 2, which also includes the identification of and preliminary justification for several simplifications used to obtain the analytical solutions shown in section 3. Section 4 interprets the results in terms of traditional energy transfer principles, explains the temporal and spatial behavior of the stabilization process, and compares the results to independent numerical evidence to establish the validity of the simplifications used in section 2. Section 5 explains the basis for the forced transient adjustment in the numerical models in terms of the unforced transient adjustment analyzed herein. Section 6 briefly discusses the principal results of this work and the potential role of the barotropic stability mechanism in baroclinic vortex dynamics.

2. The analytical model

a. Background

The motivation for the following analytical development is the study of NDBT f-plane Couette flow by Case (1960). He obtained an integral solution for the time evolution of linear perturbations imposed as initial conditions on the NDBT Couette flow, which is a steady, zonally uniform flow with constant latitudinal shear (Fig. 1a). Case's result may be interpreted as an infinite summation of a continuum of singular solutions, hereafter referred to as continuous spectrum modes (Pedlosky 1964). For the NDBT f-plane Couette flow problem, this continuous spectrum forms a complete basis, since discrete normal modes are eliminated by the lack of an environmental vorticity gradient. The superposition of these continuous spectrum modes re-

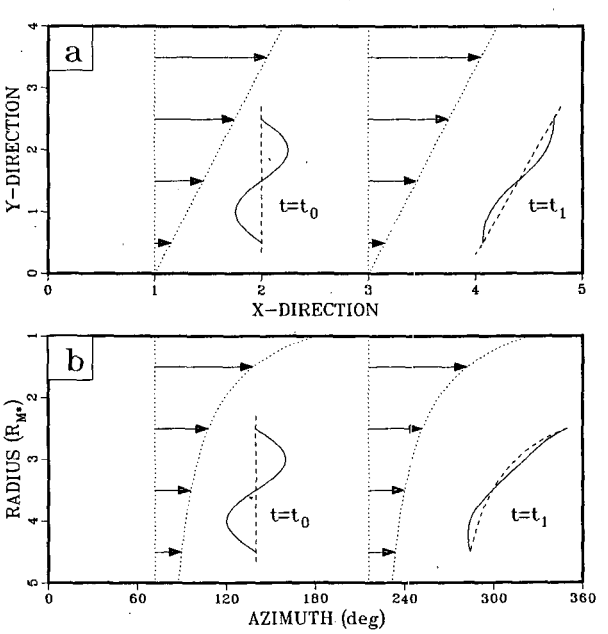

FIG. 1. Schematic portrayal of perturbation damping with time due to (a) a meridionally sheared Couette flow, and (b) a radially sheared axisymmetric vortical flow.

sults in a perturbation streamfunction structure that has an algebraic time dependence (i.e., depends on factors involving t to an integer power) as the perturbation is tilted down-shear by the Couette flow. Although the baroclinic Couette flow study of Farrell (1982) showed that initial growth of the perturbation is possible for particular initial conditions, both Farrell (1982) and Case (1960) showed that the response is asymptotically proportional to t^{-2} for $t \to \infty$, as schematically portrayed in Fig. 1a. In terms of instability theory, NDBT f-plane Couette flow may be viewed as a barotropically stable "basic state" with respect to linear perturbations.

The NDBT f-plane Couette flow model, as in the Eady or Charney models, may be viewed as an idealization of the response of synoptic disturbances to a particular planetary-scale flow. Along with other limitations, the accuracy of this approach depends on the extent to which synoptic-scale disturbances may be regarded as linear perturbations. In the case of an intense vortex such as a tropical cyclone, such an assumption would be clearly unjustified since the TC winds can be substantially stronger than the environmental flow at quite large distances from the center. The large magnitude and nearly circular structure of the TC windfield suggests, however, that a model analogous to NDBT f-plane Couette flow could be developed in a polar coordinate system moving with the center of the TC. In such a model, the axisymmetric component of the TC outside the radius of maximum winds (R_{M^*}) may be regarded as a radially sheared NDBT "basic state" that is time-invariant in the moving reference frame, and the asymmetric component of the vortex may be regarded as a perturbation to the symmetric basic state. If the axisymmetric basic state has constant vorticity, then an initial perturbation can be expected to damp completely as it is tilted in the direction of the symmetric radial shear (Fig. 1b). A vortex model based on a constant vorticity basic state and initial perturbations is clearly a special case, and the implications of such approximations will be addressed explicitly as the analysis proceeds.

b. Model development

The behavior of fluid motion in a NDBT system on a β-plane is described by

$$\frac{\partial \zeta}{\partial t} + \mathbf{V} \cdot \nabla(\zeta + f) = 0 \tag{1}$$

$$\zeta = \mathbf{k} \cdot \nabla \times \mathbf{V} \tag{2}$$

$$f = f_0 + \beta y, \tag{3}$$

where ζ is the local vertical component of relative vorticity, β is the linearized latitudinal derivative of the Coriolis parameter f, and f_0 is the average value of f in the domain. Since a perturbed vortex generally will not remain stationary, a transformation to a reference frame moving with the center of the symmetric vortex component (defined below) must be accomplished to take advantage of the near-axisymmetry of the vortex (e.g., Willoughby 1988). The following differentiation relationships apply:

$$\nabla = \nabla' \tag{4}$$

$$\frac{\partial}{\partial t} = \frac{\partial'}{\partial t} - \mathbf{C} \cdot \nabla', \tag{5}$$

where $\mathbf{C}(t)$ is the velocity of the moving reference frame and the ($'$) symbol denotes operations with respect to coordinates in the moving reference frame. Such a transformation permits the fluid to be conveniently partitioned into three parts,

$$\mathbf{V} = \mathbf{V}_S + \mathbf{V}_E + \mathbf{V}_A, \tag{6}$$

according to the following definitions: (i) $\mathbf{V}_S$ is a known symmetric (S) cyclone component that is steady in the moving reference frame; (ii) $\mathbf{V}_E$ is a known zonal environmental (E) flow that depends only on latitude and is steady in the stationary reference frame; and (iii) $\mathbf{V}_A$ is an asymmetric (A) flow component that represents unknown perturbations to the symmetric cyclone produced by the environmental and vortex processes discussed in section 1. Subject to these definitions, substituting (4)–(6) into (1)–(3) gives

$$\frac{\partial' \zeta_A}{\partial t} + (\mathbf{V}_S + \mathbf{V}_E - \mathbf{C}) \cdot \nabla' \zeta_A + (\mathbf{V}_A - \mathbf{C}) \cdot \nabla' \zeta_S + \mathbf{V}_A \cdot \nabla'(\zeta_A + \zeta_E + f') = -\mathbf{V}_S \cdot \nabla'(\zeta_E + f') - \mathbf{V}_E \cdot \nabla' \zeta_S, \tag{7}$$

in which the various terms have been grouped so that the left side represents a nonlinear partial differential equation in terms of the perturbation flow. The terms on the right side of (7) represent forcing processes that act to generate ζ_A. The terms $\mathbf{V}_S \cdot \nabla' \zeta_S$ and $\mathbf{V}_E \cdot \nabla' \zeta_E$ are absent because $\mathbf{V}_S$ and $\mathbf{V}_E$ are orthogonal to their respective vorticity gradients. It is important to note that in (7) a convention of leaving the dependent variables untransformed has been employed. Although relative vorticity and the gradient of the Coriolis parameter are invariant with respect to the coordinate transformation, fluid velocity is not. Thus, the convention results in explicit advection by $\mathbf{C}$ in (7), but has the desirable property of avoiding an implicit dependence of the perturbation flow $\mathbf{V}_A$ on $\mathbf{C}$. Such a convention is necessary to justify the use of the homogeneous boundary conditions that will be employed in this model.

To transform (7) into an unforced problem, the explicit dependence on environmental wind and variable f is removed to give

$$\frac{\partial \zeta_A}{\partial t} + \mathbf{V}_S \cdot \nabla \zeta_A + (\mathbf{V}_A - \mathbf{C}) \cdot \nabla \zeta_S + (\mathbf{V}_A - \mathbf{C}) \cdot \nabla \zeta_A = 0, \tag{8}$$

in which the (′) symbols have been omitted for clarity. In all subsequent analysis, independent variables will be relative to the moving coordinate system. Equation (8) describes the evolution of an asymmetric perturbation initially imposed on a symmetric basic state vortex in a quiescent environment and on an f-plane. With the addition of two homogeneous boundary conditions at specified radii, (8) becomes the homogenous counterpart to (7) over the enclosed domain. Since an assumption of linearity will be imposed later in the development [i.e., $(\mathbf{V}_A - \mathbf{C})\cdot\nabla\zeta_A$ is negligible], linear differential equation theory can be employed to show that certain relationships exist between the free-perturbation response and the forced-perturbation response. This issue will be specifically addressed in section 5a within the context of the free-perturbation behavior illustrated in section 3.

The model development is continued by imposing a polar coordinate system on the moving reference frame. In this system

$$\mathbf{V}_S = v_S(r)\Theta, \tag{9a}$$

$$\mathbf{V}_A = u_A(r, \theta, t)\mathbf{r} + v_A(r, \theta, t)\Theta, \tag{9b}$$

$$\mathbf{C} = C[\cos(\theta - \alpha)\mathbf{r} - \sin(\theta - \alpha)\Theta], \tag{9c}$$

where $\mathbf{r}$ and Θ are unit vectors in the radial and azimuthal directions, respectively, and $\mathbf{C}$ and α are the speed and direction of the coordinate system motion, respectively. The mathematical convention of measuring angles counterclockwise from east has also been used. Substituting (9a, b, c) into (8) gives

$$\underset{\text{(a)}}{\frac{\partial\zeta_{A^*}}{\partial t_*}} + \underset{\text{(b)}}{\frac{v_{S^*}}{r_*}\frac{\partial\zeta_{A^*}}{\partial\theta}} + \underset{\text{(c)}}{[u_{A^*} - C_*\cos(\theta - \alpha)]\frac{\partial\zeta_{S^*}}{\partial r_*}} + \underset{\text{(d)}}{(\mathbf{V}_{A^*} - C_*)\cdot\nabla\zeta_{A^*}} = 0, \tag{10}$$

in which asterisked subscripts have been employed to denote dimensional variables. In all subsequent analysis, the absence of an asterisk will denote nondimensional variables.

The advection of perturbation vorticity by the radially variable symmetric flow in term (b) of (10) is analogous to the shearing process that causes perturbation damping in the Couette flow model. In addition to manifesting vortex motion through the advection of symmetric vorticity, term (c) permits the propagation of neutral and possibly exponentially growing discrete normal modes on the radial gradient of ζ_{S^*}. This term represents a serious obstacle to an analytical solution approach since ζ_{S^*} has a strong radial dependence that varies with the particular vortex structure specified. Thus, to facilitate analysis of the damping process associated with term (b), term (c) will be removed by (i) requiring that v_{S^*} have a Rankine radial dependence over a horizontal area bounded on the inside by the radius of maximum winds (R_{M^*}), and (ii) limiting the domain of the imposed perturbation to that region. To facilitate specification of initial conditions in section 2c, the modified Rankine profile (see Anthes 1982, p. 22) will be used:

$$v_{S^*} = \mathbf{V}_{M^*}\left(\frac{R_{M^*}}{r_*}\right)^X, \quad r_* \geq R_{M^*}, \tag{11}$$

where V_{M^*} is the magnitude of the symmetric windspeed for $r_* = R_{M^*}$. The Rankine profile is the limiting value of (11) as $X \to 1$.

Choosing v_{S^*} to be Rankine not only eliminates any discrete normal mode components from linear solutions to (10), but also may have a significant impact in the continuous spectrum response. Both these issues must be addressed before the results of this model can be used to interpret the numerical studies cited earlier that used non-Rankine vortices. The impact on the continuous spectrum can be assessed by drawing an analogy between (10) and NDBT Couette flow on a rotating sphere in the sense that the radial gradient of ζ_{S^*} has an influence analogous to the latitudinal variation of the Coriolis parameter. For a β-plane approximation, Kao (1955) and Boyd (1983) have shown that β_* has no influence on the rate of continuous spectrum damping, but rather causes the continuous spectrum wave to retrogress proportional to β_* in a manner related to the familiar discrete mode propagation. Because the retrogression is independent of latitude for a constant β_*, the damping rate depends only on the magnitude of the Couette flow shear. Since the radial gradient of ζ_{S^*} is inward in the inner part of a typical vortical flow and decreases rapidly with increasing radius, it is anticipated that a continuous spectrum wave will retrogress (i.e., clockwise for a cyclonic vortex) faster at smaller radii than it would at larger radii. The result would be slower damping since the retrogression would tend to counter the tilting induced by v_{S^*}. This effect should be negligible for any modified Rankine vortical flow with $X \approx 1$. The numerical results of McCalpin (1987) cited in section 4b will indicate that significant perturbation retrogression can occur for a vortex that has a large highly variable symmetric vorticity gradient. Comparison of the results of this model with those of FE and DM, however, will suggest that the symmetric vorticity gradient of a tangential wind profile that approximates a TC causes only minor slowing of perturbation damping due to variable retrogression. Analysis of McCalpin's results will also suggest that virtually no energy from an initial perturbation projects onto any discrete modes. Thus, the use of a Rankine vortex will be shown to be reasonable for analysis of unforced perturbation responses.

Understanding the constraints on linearizing (10), and comparing solutions to this model with related

work, will be facilitated by nondimensionalizing (10) and (11) using the relationships

$$r_* = R_{M^*} r, \quad v_{S^*} = V_{M^*} v_S, \quad t_* = \frac{R_{M^*}}{V_{M^*}} t$$

$$\zeta_{A^*} = Z_{A^*} \zeta_A, \quad \mathbf{V}_{A^*} = Z_{A^*} R_{M^*} \mathbf{V}_A, \quad C_* = Z_{A^*} R_{M^*} C,$$

where Z_{A^*} is the maximum of the initial perturbation vorticity. This nondimensionalization gives

$$\frac{\partial \zeta_A}{\partial t} + \omega_S \frac{\partial \zeta_A}{\partial \theta} + \epsilon(\mathbf{V}_A - \mathbf{C}) \cdot \nabla \zeta_A = 0, \quad r \geq 1 \quad (12a)$$

$$\omega_S \equiv \frac{v_S}{r} = \frac{1}{r^2}, \quad (12b)$$

where ω_S is the symmetric angular wind. The additional parameter ϵ provides a measure of linearity and is defined by

$$\epsilon = \frac{Z_{A^*}}{V_{M^*}/R_{M^*}}. \quad (13)$$

In principle, (12a) can be made linear over an arbitrarily large domain by specifying ϵ to be "sufficiently small." In practice, the anisotropic radial dependences of the symmetric angular wind and the various initial perturbations developed in Section 2b make it difficult to determine a priori an upper bound on ϵ to insure (12a) will be reasonably linear for a particular domain and time period. It will be assumed that requiring $\epsilon \leq 0.1$ and $r \leq 10$ will be adequate to keep the model reasonably linear. With the nonlinear term removed, (12a) represents a polar coordinate equivalent to NDBT f-plane Couette flow.

The model may now be solved by defining a perturbation streamfunction

$$\mathbf{V}_A = \mathbf{k} \times \nabla \psi_A, \quad \zeta_A = \nabla^2 \psi_A, \quad (14a,b)$$

assigning homogeneous boundary conditions

$$\psi_A(a, \theta, t) = \psi_A(b, \theta, t) = 0, \quad (15a,b)$$

to confine the perturbation to the desired domain $a = 1$, $b = 10$, and removing the azimuthal dependence using the Fourier series

$$\psi_A(r, \theta, t) = \mathrm{Re}\{\sum_{k=1}^{\infty} \Psi^k(r, t) e^{ik\theta}\}. \quad (16)$$

Substituting (14b) and the k^{th} term of (16) into a linear (12a) and integrating with respect to time gives

$$\left[\frac{\partial^2}{\partial r^2} + \frac{1}{r}\frac{\partial}{\partial r} - \frac{k^2}{r^2}\right] \Psi^k(r, t) = \zeta_0{}^k e^{-ikt\omega_S} \quad (17a)$$

$$\zeta_0{}^k \equiv \left[\frac{\partial^2}{\partial r^2} + \frac{1}{r}\frac{\partial}{\partial r} - \frac{k^2}{r^2}\right] \Psi^k(r, 0). \quad (17b)$$

Substituting (16) into (15a, b) gives

$$\Psi^k(a, t) = \Psi^k(b, t) = 0. \quad (17c,d)$$

In (17c,d) $\zeta_0{}^k$ is the radial structure of the azimuthal wavenumber k component of the initial asymmetric vorticity. Hereafter, the term "wavenumber" will mean "azimuthal wavenumber" unless stated otherwise.

Equations (17a–d) constitute a fully specified boundary value problem. The solution may be formally written in terms of a Green's function:

$$\Psi^k(r, t) = \int_a^b G(r, \rho) \zeta_0{}^k(\rho) e^{-ikt\omega_S(\rho)} d\rho. \quad (18)$$

Using standard techniques (Case 1960), the Green's function is calculated to be

$$G(r, \rho) = \begin{cases} \dfrac{a^{2k} - r^{2k}}{2kr^k(a^{2k} - b^{2k})} (\rho^{k+1} - b^{2k}\rho^{-k+1}), & a \leq r \leq \rho \\ \dfrac{b^{2k} - r^{2k}}{2kr^k(a^{2k} - b^{2k})} (\rho^{k+1} - a^{2k}\rho^{-k+1}), & \rho \leq r \leq b. \end{cases} \quad (19)$$

Finally, substituting (18) into (16) gives

$$\psi_A(r, \theta, t) = \mathrm{Re}\left\{\sum_{k=1}^{\infty} \int_a^b G(r, \rho) \zeta_0{}^k(\rho) e^{-ik(\theta - t\omega_S(\rho))} d\rho\right\}, \quad (20)$$

which represents a formal solution for the time evolution of the perturbation streamfunction. Although exact solutions to (20) do exist for certain initial conditions, the integral generally must be evaluated numerically. A simple trapezoidal scheme will be used.

c. *Initial condition specification*

To evaluate (20), an appropriate functional form for $\zeta_0{}^k$ and magnitude for Z_{A^*} must be specified. It is not immediately clear what combination of radial and azimuthal dependences to associate with asymmetries generated by the vortex-environment interactions identified in section 1. The right side of (7) is used for this purpose by writing in dimensional form

$$\frac{\partial \zeta_{A^*}}{\partial t_*} \propto \underbrace{-v_{S^*}\left(\frac{\partial \zeta_{E^*}}{\partial y_*} + \beta_*\right)\cos\theta}_{(a)} - \underbrace{(u_{E^*} - c_{X^*})\frac{\partial \zeta_{S^*}}{\partial r_*}\cos\theta}_{(b)} + \underbrace{c_{Y^*}\frac{\partial \zeta_{S^*}}{\partial r_*}\sin\theta}_{(c)}, \quad (21)$$

where u_{E^*} is the zonal component of the environmental wind and $c_{X^*} \equiv C_* \cos\alpha$ and $c_{Y^*} \equiv C_* \sin\alpha$ are the zonal and meridional components of the coordinate

system velocity, respectively. Advection by C_* is present because the term $-\mathbf{C}_* \cdot \nabla\zeta_{S^*}$ from the left side of (7) has been included in (21) to properly reflect that the generation of asymmetries from symmetric vorticity depends on the difference between vortex motion and the environmental wind (cf. Willoughby 1988). To determine the spatial structure of the forcing terms in (21), first let u_{E^*} be approximated by a truncated Taylor series expansion in y_* about the present position of the symmetric cyclone center

$$u_{E^*}(y_*) = u_{E^*}(0) + S_{E^*} y_* - \frac{1}{2}\beta_{E^*} y_*^2 \quad (22a)$$

$$S_{E^*} \equiv \left.\frac{\partial u_{E^*}}{\partial y_*}\right|_{y_*=0}, \quad \beta_{E^*} \equiv -\left.\frac{\partial^2 u_{E^*}}{\partial y_*^2}\right|_{y_*=0}, \quad (22b,c)$$

where S_{E^*} and β_{E^*} are the shear in the environmental wind and the latitudinal derivative of the environmental relative vorticity respectively, which are evaluated at the center of the symmetric vortex. Second, let the radial gradient of symmetric vorticity be written in terms of (11). Now a Rankine profile ($X = 1$) has zero vorticity as desired to delete term (c) from (10). As noted in section 2b, a small perturbation away from $X = 1$ may also be considered as a valid model extension since the radial shear of v_S would be essentially unchanged, and the associated damping should be little affected by the small radial gradient of ζ_{S^*} that would be introduced. Thus, using (11) with $X \approx 1$ gives

$$\frac{\partial\zeta_{S^*}}{\partial r_*} \approx (X^2 - 1)\frac{V_{M^*}R_{M^*}}{r_*^3}. \quad (23)$$

Considering only term (a) of (21), substituting (11) and (22a) gives

$$\frac{\partial\zeta_{A^*}}{\partial t_*} \propto \frac{-V_{M^*}R_{M^*}}{r_*}(\beta_* + \beta_{E^*})\cos\theta, \quad (24)$$

which represents the generation of a wavenumber 1 asymmetry from the advection of absolute vorticity ($\beta_* + \beta_{E^*}$) by the symmetric vortex. A nondimensional initial condition with equivalent spatial structure (hereafter referred to as a "β-induced asymmetry") for use in this unforced model would be

$$\zeta_0{}^k(r) = \frac{-1}{r}, \quad k = 1. \quad (25)$$

The quantity ($\beta_* + \beta_{E^*}$) is assumed positive corresponding to a poleward gradient of environmental absolute vorticity. Such asymmetries represent the large gyres that have been identified in numerical models (FE) and in observations (Chan 1986).

Considering only term (b) of (21), substituting (23) and only the two lowest order terms from (22a) gives

$$\frac{\partial\zeta_{A^*}}{\partial t_*} \propto (1 - X^2)V_{M^*}R_{M^*} \times \left[\frac{(u_{E^*}(0) - c_{X^*})}{r_*^3}\cos\theta + \frac{S_{E^*}}{2r_*^2}\sin 2\theta\right], \quad (26)$$

in which the identities $y_* \equiv r_* \sin\theta$ and $2\sin\theta\cos\theta \equiv \sin 2\theta$ have been used. The right side of (26) represents the generation of a wavenumber 1 asymmetry due to vortex motion relative to the environment, and a wavenumber 2 asymmetry due to linear shearing of symmetric vorticity by the relative environmental wind. Appropriate initial conditions for this model (hereafter referred to as "motion-induced" and "shear-induced" asymmetries, respectively) would be

$$\zeta_0{}^k(r) = \frac{1}{r^3}, \quad k = 1, \quad (27)$$

$$\zeta_0{}^k(r) = \frac{-i}{r^2}, \quad k = 2. \quad (28)$$

It has been assumed that (i) X is slightly less than 1 to give the symmetric vortex cyclonic vorticity; (ii) S_{E^*} is positive corresponding to anticyclonic shear equatorward of the subtropical ridge; and (iii) the quantity $[u_{E^*}(0) - c_{X^*}]$ is positive, which corresponds to the generally westward movement of TCs relative to environmental steering documented by composite studies (Chan and Gray 1982; Holland 1984). Term (c) of (21) will not be used, since it would result in an initial condition identical to (28) except for the phase.

It is inappropriate in this simple model to assign an individual perturbation vorticity scale Z_{A^*} to each of the above initial conditions based on the scales of the associated forcing terms. Instead, all but one of the following model solutions will use a value for Z_{A^*} such that $\epsilon = 0.1$ according to (13) to facilitate analyzing the dependence of vortex stability on perturbation spatial structure. The radial structures of the four initial perturbations defined above are shown in Fig. 2.

3. Model results

a. Perturbation damping

Before numerically evaluating (20) using the initial conditions developed above, it is useful to obtain exact solutions by choosing initial conditions of the form

$$\zeta_0{}^k(r) = \frac{1}{r^{k+4}}. \quad (29)$$

An asymmetry of this type may be viewed as an approximation to the wavenumber k component of a perturbation produced by localized asymmetric convection in a TC eyewall cloud (hereafter refered to as a "convection-induced asymmetry"). Initial condition (29) for $k = 1$ and $k = 2$ is also shown in Fig. 2, and results in solutions to (20) of

$$\psi_A(r, \theta, t) = \frac{1}{4t^2}\left[\frac{a^2(r^2 - b^2)}{r(a^2 - b^2)}\cos(\theta - t/a^2) + \frac{r^2(b^2 - a^2)}{r(a^2 - b^2)}\cos(\theta - t/r^2) + \frac{b^2(a^2 - r^2)}{r(a^2 - b^2)}\cos(\theta - t/b^2)\right] \tag{30}$$

and

$$\psi_A(r, \theta, t) = \frac{1}{16t^2}\left\{\frac{a^4(r^4 - b^4)}{r^2(a^4 - b^4)}\left[\frac{1}{a^2}\cos2(\theta - t/a^2) + \frac{1}{2t}\sin2(\theta - t/a^2)\right]\right.$$
$$+ \frac{r^4(b^4 - a^4)}{r^2(a^4 - b^4)}\left[\frac{1}{r^2}\cos2(\theta - t/r^2) + \frac{1}{2t}\sin2(\theta - t/r^2)\right]$$
$$\left. + \frac{b^4(a^4 - r^4)}{r^2(a^4 - b^4)}\left[\frac{1}{b^2}\cos2(\theta - t/b^2) + \frac{1}{2t}\sin2(\theta - t/b^2)\right]\right\}, \tag{31}$$

respectively.

Both (30) and (31) damp algebraically with time as is characteristic of continuous spectrum mode solutions. It should be noted that the wavenumber 2 perturbation damps four times as rapidly as the wavenumber 1 perturbation, which suggests that the damping rate is proportional to the square of perturbation wavenumber. This result is analogous to the dependence of damping on the perturbation zonal wavenumber for plane Couette flow (Case 1960). The evolution of (30) and (31) over a 2 hour period are shown in Figs. 3a–c and Figs. 3d–f respectively. Unless otherwise noted, all illustrated solutions use the following parameter specifications: $a = 1$, $b = 10$, $V_{M^*} = 50$ m s^{-1}, $R_{M^*} = 50$ km and $\epsilon = 0.1$. The contour interval is the same for each row of panels to show clearly the damping process. This comparison emphasizes the strong dependence of the damping process on perturbation wavenumber, and also clearly illustrates how the radial variability of v_S tilts the perturbations downshear.

The perturbation streamfunctions for the motion-induced and shear-induced asymmetries (not shown) undergo a similar, but slower shearing and damping process. A quantitative comparison of damping rates is facilitated by Fig. 4a, which shows the decay of perturbation kinetic energy with time for each of the four cases. Although perturbations of the same wavenumber damp at nearly the same rate initially, the damping rates quickly diverge. As will be shown in section 4a, this property is due significant differences in the radial dependences of the initial conditions, e.g., r^{-6} for a wavenumber 2 convection-induced asymmetry as compared to r^{-2} for the shear-induced asymmetry. Thus, NDBT vortex stability to asymmetric perturbations is quite sensitive to the radial as well as azimuthal structure of the perturbation.

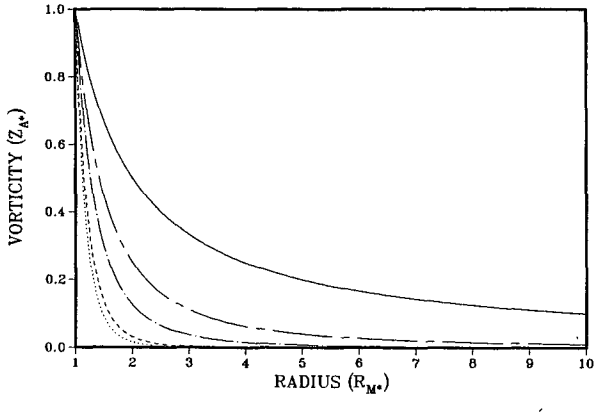

FIG. 2. Radial dependence of initial perturbation vorticity ($Z_{A^*}\zeta_0^k$) for convection-induced ($k = 2$, dot; $k = 1$, dash), motion-induced (chaindot), shear-induced (chaindash) and β-induced (solid) asymmetries.

The kinetic energy decay for a β-induced asymmetry is shown in Fig. 4b. Perturbation kinetic energy decays by approximately 80% in 24 h, which agrees quite well with the adjustment period observed in the NDBT numerical models of TC motion cited earlier. The much slower damping rate in Fig. 4b is consistent with the discussion in the preceding paragraph since the perturbation vorticity associated with a β-induced asymmetry decreases significantly slower with increasing radius than any of the previous initial conditions (Fig. 2). The evolution of both the total and perturbation streamfunction components over a 36-hour period is shown in Fig. 5. The value of ϵ has been increased to 0.5 in Fig. 5 to emphasize how an initially perturbed NDBT vortex is restored to axisymmetry. By 8 h, the inner part of the vortex has already regained an essentially axisymmetric structure (Fig. 5b), while the outer vortex remains appreciably distorted. No analogy to this behavior exists in horizontal plane Couette flow, since the linear shear in that model renders the damping process independent of latitude.

b. Influence of boundary conditions

Boundary conditions (15a, b) were chosen to facilitate development of the model and are clearly nonphysical. Thus, it is important to determine the extent to which the boundary conditions may have influenced the results presented above. Two aspects of this problem must be addressed.

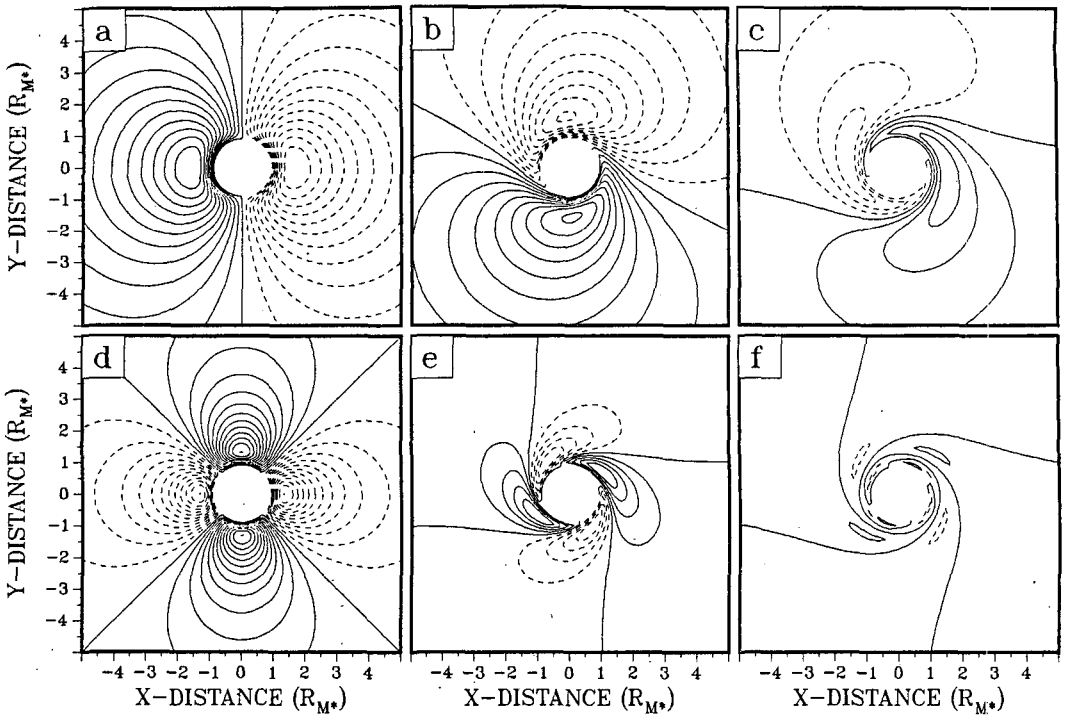

FIG. 3. (a)-(c) Perturbation streamfunction (solid, positive; dashed, negative) for a $k = 1$ convection-induced asymmetry at $t = 0$, 1 and 2 hours, respectively. Contour interval is 9.6×10^2 m^2 s^{-1}. (d)-(f) Same as (a)-(c) except for a $k = 2$ convection-induced asymmetry, and a contour interval of 4.3×10^2 m^2 s^{-1}.

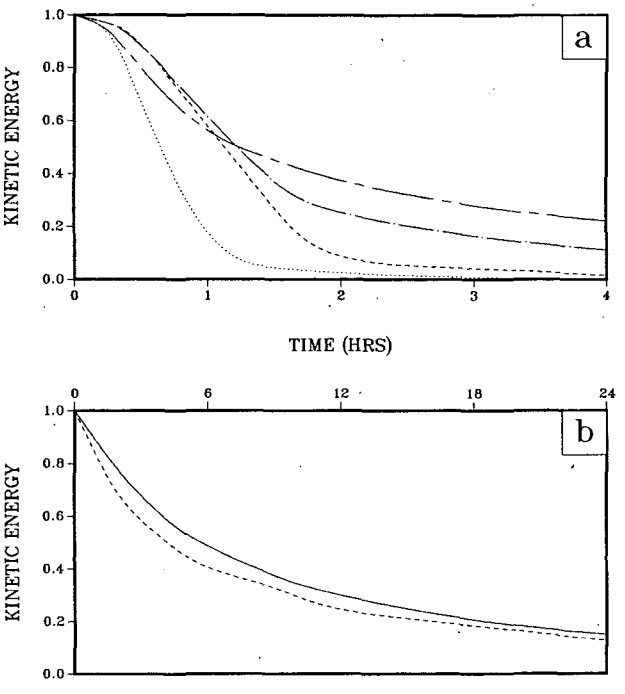

FIG. 4. (a) Decay of perturbation kinetic energy (normalized by initial value) with time for convection-induced ($k = 2$, dot; $k = 1$, dash), motion-induced (chaindot) and shear-induced (chaindash) asymmetries. (b) Same as (a), except for a β-induced (solid) and a modified β-induced (dash) asymmetry.

First, boundary influences will become increasingly significant with time if there is a tendency for perturbation energy to propagate radially and cause a concentration at either boundary. This problem may be formally addressed by considering

$$\zeta_A(r, \theta, t) = \mathrm{Re}\{\zeta_0{}^k(r)e^{ik(\theta-\omega_S t)}\}, \qquad (32)$$

which is obtained by substituting (14b) and (17a, b) into the Laplacian of (16). Equation (32) indicates that perturbation vorticity is conserved following the symmetric angular wind, which is a purely azimuthal motion. This result depends on the model being linear and the symmetric vortex being Rankine, but does not depend on boundary conditions. Thus, no mechanism exists in this model to propagate perturbation energy radially, nor does an examination of Fig. 3 or Fig. 5 indicate that such a process is taking place.

Second, the presence of the inner domain boundary at the location of maximum perturbation vorticity may produce nonphysical results. A nonzero inner boundary was used because a Rankine vortex is singular at the origin. The inner boundary may be moved to the origin if the singularity is removed by modifying the wind profile to be solid body rotation at all radii less than R_{M^*}. Recall that the choice of radial structure for the various initial perturbations depends on the symmetric vortex. Thus, the radial structure for a β-induced

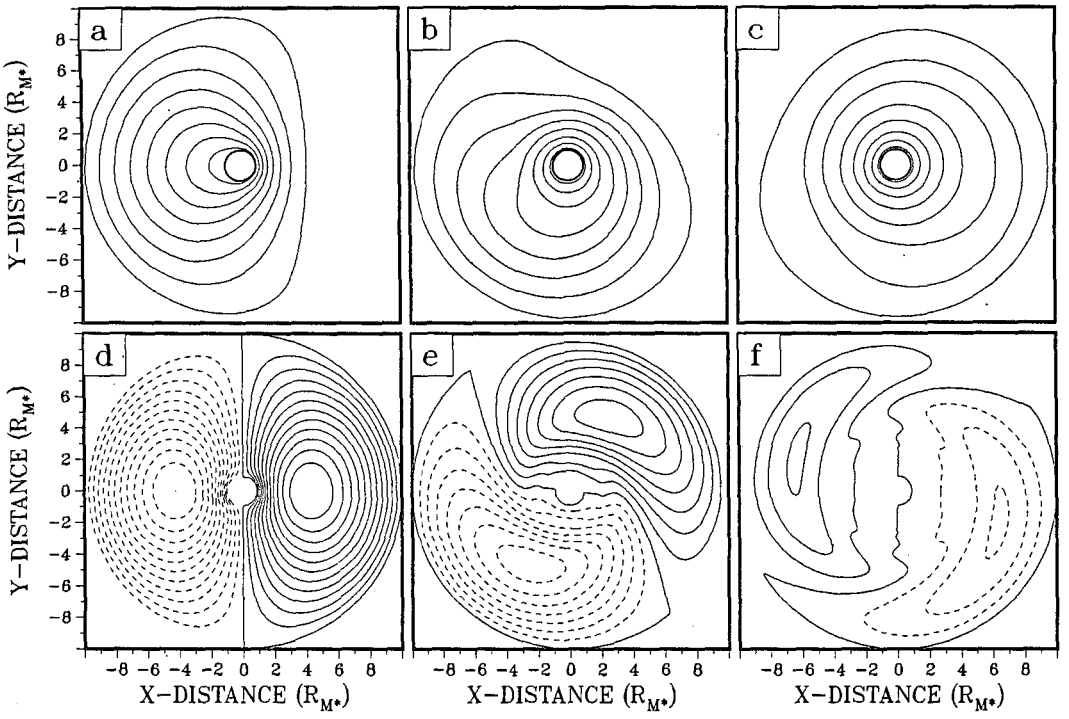

FIG. 5. (a)–(c) Perturbation plus symmetric streamfunction for a β-induced asymmetry at $t = 0$, 8 and 36 hours, respectively. Contour interval is 7.4×10^5 m^2 s^{-1}. (d)–(f) Same as (a)–(c) except showing just the perturbation streamfunction (solid, positive; dashed, negative), and using a contour interval of 1.7×10^5 m^2 s^{-1}.

asymmetry associated with a Rankine vortex altered as just suggested would be

$$\zeta_0^k(r) = \begin{cases} -r, & 0 \leq r < 1 \\ \dfrac{-1}{r}, & 1 \leq r \leq b. \end{cases} \tag{33}$$

Figure 4b shows that the kinetic energy for such an initial perturbation decays at virtually the same rate as the original β-induced asymmetry.

Modifying the symmetric wind as described above causes the radial gradient of ζ_S to be singular at $r = 1$. This singularity is equivalent to a large radial gradient of vorticity, which would tend to cause clockwise retrogression and somewhat slower damping of the continuous spectrum solution as discussed earlier. Although the present model cannot give a quantitatively precise solution for the response of a perturbation to a Rankine vortex with solid body inner rotation, the response of the model to (33) is useful for demonstrating that solutions are not unduly sensitive to the location of the inner boundary.

4. Model interpretation

a. *The stabilization mechanism*

Within the context of fluid dynamical instability theory, the present stability of a linear perturbation with respect to some basic state may be assessed by computing the domain-averaged local time tendency of perturbation energy. For the particular boundary conditions used in this model, the familiar NDBT result is that domain-averaged perturbation kinetic energy must be presently increasing (decreasing) with time if the perturbation tilts against (with) the horizontal shear of the basic state. Such a result is readily obtainable for this model by substituting (14b) into (12a) with the nonlinear term omitted, multiplying by ψ_A, integrating over the domain, and performing a number of integrations by parts. Using (14a), the result may be expressed as

$$\frac{\partial E}{\partial t} = -\int_a^b \overline{(v_A u_A)} \frac{\partial \omega_S}{\partial r} r^2 dr \tag{34a}$$

$$E \equiv \int_a^b \frac{1}{2} \overline{(u_A^2 + v_A^2)} r dr \tag{34b}$$

$$\overline{(\ )} \equiv \frac{1}{2\pi} \int_0^{2\pi} (\ ) d\theta. \tag{34c}$$

Equation (34a) is analogous to the familiar result for stationary Cartesian coordinates (e.g., Farrell 1987), except that in this case it is the shear of the axisymmetric *angular* wind that controls the energy transfer process. In (34a), a positive correlation develops between the perturbation momentum flux and the symmetric angular wind shear when initially "upright"

perturbations are tilted downshear. Since the radial shear of ω_S is negative for a cyclone, the average perturbation momentum flux must also be negative. This flux represents an inward transport of cyclonic momentum that tends to accelerate the symmetric basic state at the expense of asymmetric perturbation kinetic energy.

Because the analysis thus far has been strictly linear, the symmetric vortex has been regarded as steady in the moving reference frame. Using the azimuthal momentum equation and (34c), however, the influence of perturbation momentum flux on the symmetric basic state is described by

$$\frac{\partial v_S}{\partial t} = -\epsilon^2 \overline{(u_A \zeta_A)}. \tag{35}$$

This expression may be evaluated to lowest order in ϵ using (20) and (32), and then integrated with respect to time to give

$$\Delta v_S = \frac{\epsilon^2}{2r} \zeta_0^k(r) \int_a^b \frac{G(r,\rho)\zeta_0^k(\rho)}{\omega_S(r) - \omega_S(\rho)} \times [\cos kt(\omega_S(\rho) - \omega_S(r)) - 1]d\rho, \tag{36a}$$

$$\Delta v_S(r,t) \equiv v_S(r,t) - v_S(r,0). \tag{36b}$$

The time evolution of Δv_S is illustrated in Fig. 6 using the same initial condition as in Fig. 5 except that ϵ has been reduced to 0.1, which corresponds to a more realistic asymmetric windspeed of approximately 2.8 m s^{-1} near the domain center. Although a nearly complete transfer of perturbation kinetic energy occurs by 48 h, the majority of the transfer has taken place by 24 h as anticipated from the damping rate in Fig. 4b. The domain-averaged sign of Δv_S is positive as required, but a slight decrease is evident for $r \gtrsim 6$. Interestingly, the radius at which Δv_S changes sign corresponds precisely with the maximum in perturbation streamfunction at any time (see Fig. 5f). It is also evident that the energy transfer begins initially at small radii and spreads outward with time. This aspect will be explained later in this subsection.

The momentum flux associated with the convection-induced, motion-induced and shear-induced asymmetries (not shown) had a similar impact on the symmetric basic state, with the changes in Δv_S becoming smaller, more concentrated at small radii and occurring over a shorter period of time for an initial condition that decreases more rapidly with radius. The extent to which perturbation flux tends to alter the basic state is one measure of model linearity. Thus, the results here show that the assumptions made in section 2b ($\epsilon \leq 0.1$, $r \lesssim 10$) were reasonable. This demonstration of how perturbation flux transfers energy to the symmetric vortex will be particularly useful in section 5b for understanding how a barotropic vortex achieves a quasi-steady asymmetric structure in the presence of steady asymmetric forcing.

The availability of exact solutions to this model permits valuable insights into the local dynamics of the

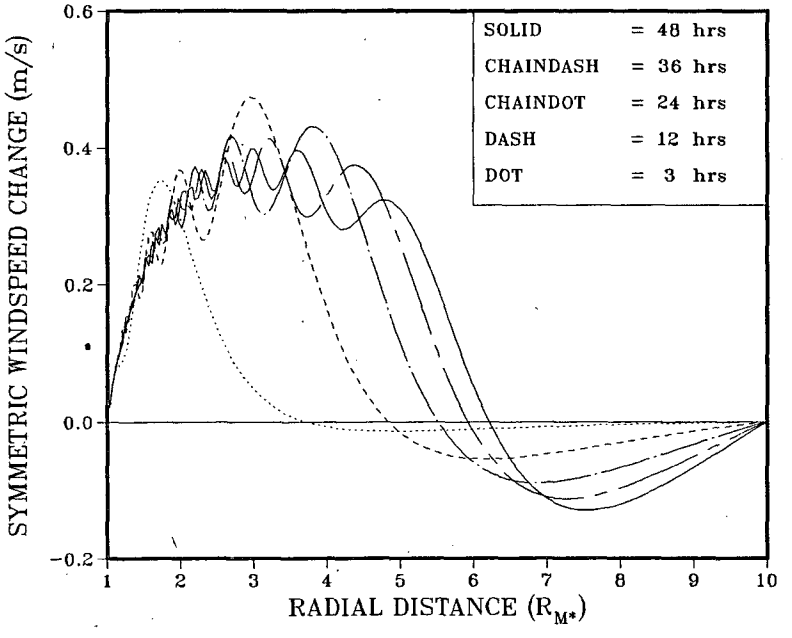

FIG. 6. Change in symmetric vortex windspeed with time (see legend) as a function of radius due to a convergence of momentum flux associated with a β-induced asymmetry. The windspeed of the mean symmetric vortex is 50 m s^{-1} at the radius of maximum winds and decreases with inverse dependence on radius to 5 m s^{-1} at 10 times the radius of maximum winds.

stability process that are not readily evident from the domain-averaged analysis conducted above. Note that by virtue of the identity

$$\nabla^2[r^{\pm k}e^{ik(\theta+\phi(t))}] \equiv 0, \tag{37}$$

the first and third terms on the right side of (30) and (31) have no vorticity, and thus are necessary solely to satisfy the boundary conditions. Therefore, substituting either of the exact solutions into (14b) results in a form

$$\zeta_A(r, \theta, t) = \nabla^2 \operatorname{Re}\{A(r, t)e^{ik(\theta-\omega_S t)}\}, \tag{38}$$

where $A(r, t)$ is an appropriate amplitude function based on the second term on the right side of either (30) or (31). Since ω_S is a function of radius, (38) will include an explicit time dependence in some of the terms associated with radial derivatives of the Laplacian. For sufficiently large t, only the term possessing the highest order explicit dependence on t needs to be retained, which produces

$$\zeta_A(r, \theta, t) \approx -\operatorname{Re}\left\{\left[\left(kt\frac{\partial\omega_S}{\partial r}\right)^2 + \left(\frac{k}{r}\right)^2\right]A(r, t)e^{ik(\theta-\omega_S t)}\right\}, \tag{39}$$

in which the term generated by the azimuthal derivatives in the Laplacian has been retained for comparison. Note that the expression k/r inside the brackets represents the inverse of the perturbation azimuthal length scale at radius r. If the first term in brackets is treated similarly, and the length scales are defined as

$$L_\theta = \frac{r}{k}, \quad L_R = 1\Big/kt\frac{\partial\omega_S}{\partial r}, \tag{40a,b}$$

then (39) may be expressed as

$$\zeta_A(r, \theta, t) \approx -\operatorname{Re}\left\{\left[\frac{A(r, t)}{L_R{}^2} + \frac{A(r, t)}{L_\theta{}^2}\right]e^{ik(\theta-\omega_S t)}\right\}. \tag{41}$$

The local dynamics of the damping process may be explained in terms of (41) as follows. Under the influence of the radial shear of ω_S, the radial length scale of the perturbation at any point in the domain exhibits an inverse dependence on t, while the azimuthal length scale remains unaltered. Since this model conserves perturbation vorticity, the left side of (41) maintains a constant magnitude. A continuing decrease in L_R thus requires the amplitude of the perturbation streamfunction to decrease proportional to t^{-2} so that the right side of (41) maintains a constant magnitude. This constraint may also be argued conceptually from the viewpoint that vorticity is a velocity change over some length scale. If the length scale is decreasing, then the velocity change must also decrease to conserve vorticity. This process, which is a time sequence of perturbation vorticity using (32) with a β-induced initial asymmetry, is shown in Fig. 7. The reduction in the radial length scale due to the shearing process is clearly illustrated by the decreasing radial spacing of the isolines of vorticity with time.

The results in section 3 show that vortex stability to asymmetric perturbations is strongly dependent on the spatial structure of the initial perturbation. From (40b), this behavior can be associated with two factors that influence L_R's inverse dependence on t. The first is the perturbation wavenumber k, which results in perturbations with a higher wavenumber damping faster than those with a low wavenumber, if the radial structures are similar. This is the case for the wavenumber 1 and 2 convection-induced asymmetries (Fig. 3), which differ little in radial dependence (Fig. 2). The second factor in (40b) is the radial shear of the symmetric angular wind, which is strongly dependent on radius. Thus, the shearing process reduces L_R much more rapidly in the inner part of the vortex relative to the outer regions, which explains why the perturbed vortex in Fig. 5b has achieved an essentially axisymmetric state in the inner region while the outer region remains distorted. This shearing distribution also explains why the speed of the damping process depends on the radial structure

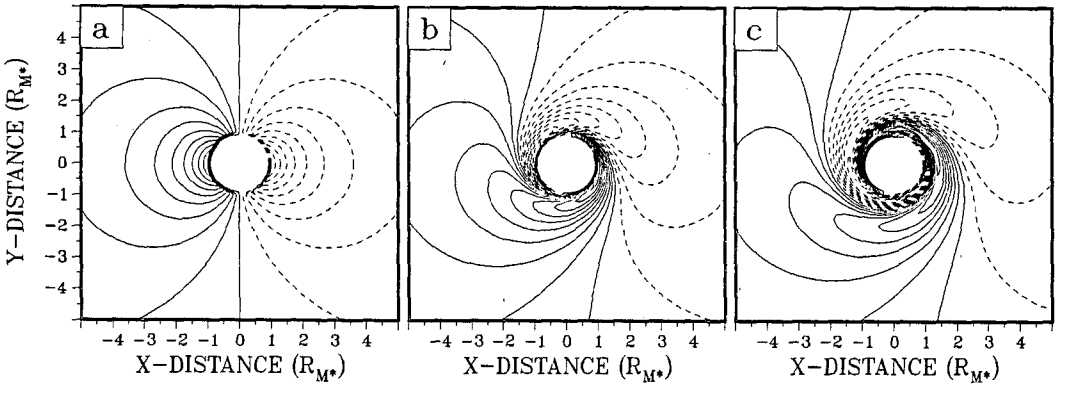

FIG. 7. (a)–(c) Perturbation vorticity (solid, cyclonic; dashed, anticyclonic) for a β-induced asymmetry at t = 0, 1 and 2 hours, respectively. Contour interval is 9.1×10^{-6} s^{-1}.

of the perturbation vorticity. An initial perturbation that decreases in magnitude more slowly with increasing radius has a greater fraction of its kinetic energy at larger radii than does a perturbation that decreases rapidly with radius. Since the radial shear of ω_S decreases rapidly with radius, it will take longer to transfer the same amount of kinetic energy from the first perturbation. Nevertheless, energy transfer still takes place rapidly near the inner boundary. This is illustrated in Fig. 6 since the symmetric vortex windspeed increases almost immediately near the inner boundary and is followed by speed increases at larger radii with increasing time.

b. *Verification with independent numerical results*

Insight into the impact of using a Rankine basic state vortex in this model can be gained by comparing the present results with a similar model that uses a non-Rankine vortex. McCalpin's (1987) quasi-geostrophic reduced-gravity numerical model of an initially perturbed ocean eddy will be used for this purpose. The difference between the dynamical frameworks of the two models is not a significant issue since this NDBT model can be readily reformulated as a quasi-geostrophic reduced-gravity model. The result is that ζ_A is replaced by perturbation potential vorticity in (12a) and that v_S becomes a K_1 exponential Bessel function having zero potential vorticity.

The main difficulty in comparing the two models is McCalpin's choice of Gaussian radial dependence for both the symmetric and asymmetric components of the eddy. Additionally, McCalpin characterized the damping of perturbation energy in terms of an exponential decay time scale, whereas the continuous spectrum response in this model is algebraic in time. Nevertheless, if the convection-induced asymmetries used here are considered to be roughly equivalent to Gaussian perturbations, then McCalpin's wavenumber 2 decay time scale of 1.5 times the symmetric flow circulation time (at the radius of maximum velocity) may be compared to the 0.8 h "exponential" time scale given by Fig. 4a for a wavenumber 2 convection-induced asymmetry. Using the 1.75 h circulation time for v_{S*} at $r_* = R_{M*}$ in this model, the damping rate here is approximately 3 times faster than in McCalpin's model. This difference is not surprising since a Gaussian vortex has an extremely strong and rapidly decreasing radial gradient of symmetric vorticity just outside R_{M*}, that should cause a significant, radially variable retrogression that can substantially reduce the rate of perturbation tilting by the symmetric flow. This assertion is supported by McCalpin's observation that perturbations were advected around the eddy at only 20% of the maximum tangential velocity. Tangential winds in a TC decay much more slowly with increasing radius than a Gaussian vortex, and thus will have a symmetric vorticity gradient that is comparatively much smaller and decreases more slowly with radius. Thus, it may be reasonably argued that the damping rates of this model better represent those associated with typical TC wind profiles. This argument is also supported by the good agreement between the 24 h adjustment period cited in NDBT numerical studies of TC motion on a β-plane and the kinetic energy transfer rates in Figs. 4b and 6. With regard to the influence of perturbation wavenumber, McCalpin's wavenumber 3 decay time scale is 2.6 times shorter than the wavenumber 2 time scale, which indicates a wavenumber dependence similar to that above.

Earlier it was noted that choosing Rankine symmetric vortex excludes potentially important discrete normal modes. When McCalpin's model was run on an f-plane, approximately 99% of the energy initially present in the imposed perturbation was transferred to the symmetric component. Such a response indicates that virtually no perturbation energy was projected onto any discrete normal modes that might exist due to the presence of a symmetric vorticity gradient. Thus, the exclusion of discrete mode processes by the choice of a Rankine vortex for this model appears justifiable for transient perturbation analysis. However, this does not rule out the potential importance of discrete modes in the steady-state component of a forced perturbation response.

5. Model application

a. *Free versus forced system relationships*

The motivation for the present modeling approach has been to exploit the analytical tractability of an unforced model for analyzing transient responses. The closed-form solutions obtained via this technique have permitted a rigorous and illuminating analysis of the perturbation damping process. To apply these results to the forced problem, it is necessary to establish what aspects of a forced-perturbation response can be reasonably inferred from the free-perturbation response.

First, it can be shown by superposition that the full solution of a linear partial differential equation with steady forcing and nonhomogeneous boundary conditions can be represented as a sum of a steady-state part that satisfies the original equation with forcing and boundary conditions, and a transient part that satisfies the homogeneous equation and that results from an initial condition that is different from the steady-state solution. Implicit in such a partitioning of the full solution is the assumption that the dynamical system actually supports a nontrivial steady-state condition. In the case of β-induced asymmetries, the NDBT numerical study of FE indicates that the asymmetric component of the vortex does tend toward a steady-state condition over the region where the symmetric vortex is significantly stronger than the asymmetric component (i.e., over the region where the present linear model is valid). Although DM did not comment

on vortex asymmetries, his illustration of a slowly varying TC motion track after 24 h indicates that vortex asymmetries associated with steady, spatially variable environmental winds also tend toward a quasi-steady state. Thus, the properties (e.g., damping time scales, azimuthal wavenumber dependence, etc.) of the unforced transient responses shown here may be expected to be relevant to the initial adjustment phase of a symmetric NDBT vortex on a β-plane with steady environmental winds.

Second, in a linear dynamical system that is first order in time and exhibits a damped transient response to steady forcing, the magnitude of the steady-state condition can be expected to be proportional to the magnitude of the forcing, but inversely proportional to the magnitude of any parameter that acts to increase the rate of transient damping. Such an assertion is formally verifiable in the case of a constant coefficient ordinary differential equation, and may be reasonably extended to NDBT vortex dynamics for situations where numerical evidence (i.e., FE; DM) confirms a damped transient response to steady asymmetric forcing. Thus, the impact of perturbation azimuthal and radial structure on the damping process in this model can be expected to influence the steady-state response to asymmetric forcing.

b. Barotropic vortex adjustment to steady forcing

The process by which vortex adjustment to steady asymmetric forcing occurs in the various NDBT simulations of TC motion (Anthes and Hoke 1975; Kitade 1981; DM; Chan and Williams 1987; FE) may be explained as follows. As the initially symmetric vortex advects planetary and environmental vorticity or is distorted by environmental wind shear and vortex motion, an asymmetric component of vortex vorticity is generated from the symmetric component as indicated in (21). This process is a transfer of kinetic energy from the symmetric vortex to the growing asymmetry. If "self-advection" (i.e., vortex flow advecting vortex vorticity) is omitted as in Chan and Williams, then the energy transfer continues unchecked and causes rapid dispersion of the vortex. The analysis in section 4a showed, however, that advection of the asymmetric vortex vorticity by the radially sheared symmetric angular wind acts to transfer perturbation energy to the symmetric vortex (Fig. 6) in this model. In the NDBT models just cited, the rate of energy transfer to the symmetric vortex apparently grows as the forced asymmetry grows until a quasi-steady balance is achieved over the region in which the symmetric vorticity is significantly greater than the asymmetric vorticity. This balance is in large measure achieved by about 24 h for asymmetries associated with vortex advection of environmental absolute vorticity (Fig. 4b), and occurs much faster for asymmetries associated with distortion of the vortex by the environment, vortex motion, or asymmetric convection (Fig. 4a). This variability in adjustment time scale for different asymmetries is due primarily to the difference in radial dependence between $v_S(r^{-1})$ and the radial gradient of $\zeta_S(r^{-3})$ from which the asymmetries are generated. Although these particular dependences are specific to a near-Rankine vortex, the principal applies generally since the symmetric vorticity gradient must decrease faster than the symmetric wind for all vortical flows that tend toward zero with increasing radius.

The steady-state phase and amplitude toward which the asymmetric structure tends clearly cannot be addressed with a homogeneous model that also excludes the potentially important influence of discrete normal modes. However, two aspects of the steady state may reasonably be inferred. First, the steady-state asymmetry will likely retain a down-shear tilt to maintain the vortex against the continuous dispersive effect of the asymmetric forcing. Such a feature was noted by FE in the structure of a β-induced asymmetry. The second inference concerns the combination of radial and azimuthal dependence that is likely to be present in the steady-state asymmetry. In the absence of environmental winds, the β-effect results in a quasi-steady vortex asymmetry that is essentially wavenumber 1 in structure (FE). As shown in section 2c, however, a horizontally variable environmental windfield will act to induce higher wavenumbers through distortion of the symmetric vortex. The spatial structure of the resultant asymmetry will depend on both the spatial structure of the environmental forcing and the dependence of the damping mechanism on perturbation structure. The authors are not aware of any detailed analyses of the wavenumber distribution and radial structure of TC asymmetries in either composite observations or model runs using realistic windfields. Thus, it is merely noted that the wavenumber and radial dependences of the stabilization mechanism shown here should contribute to the predominance of low wavenumbers and increasing axisymmetry toward the vortex center respectively.

6. Discussion and conclusion

The principal contribution of this paper has been to identify the asymmetry-damping influence of symmetric angular windshear as the mechanism by which a NDBT vortex counters dispersive and distorting influences over the region dominated by nonlinear self-advection. The present "linear" model captures the essence of the self-advection process by linearizing with respect to a nonzero symmetric basic state. In the NDBT models cited in section 5b, the asymmetry-damping mechanism acts as a negative feedback process in which a kinetic energy transfer from the asymmetric to the symmetric component of the vortex occurs as a result of, but in opposition to, the kinetic energy transfer from symmetric to asymmetric component induced by external forcing.

In the previous subsection, the stabilization mechanism was applied to the initial adjustment of a symmetric NDBT model vortex subjected to steady asymmetric forcing; however, the principle can also explain NDBT vortex adjustment to changes in the external forcing with time. For example, assume that a quasi-steady vortex asymmetry exists due to previously steady asymmetric forcing, and that a change now occurs in the environmental windfield, e.g., in β_{E^*} (24) or S_{E^*} (26). If the change is such that the magnitude of asymmetric forcing at a particular wavenumber is reduced (increased), then the shear-induced feedback of energy from the existing asymmetry to the symmetric vortex will be greater (less) than the environmentally forced transfer of energy from the symmetric vortex to the asymmetry. As a result, the vortex will adjust toward a less (more) asymmetric state at that particular wavenumber until a quasi-steady balance is reestablished. A similar adjustment process would take place if the radial distribution of the forcing at any wavenumber is altered by changes in symmetric vortex structure. If the duration of the external forcing change is brief compared to the time scale of the stabilization mechanism (i.e., approximating a step function), then the adjustment time should be on the order of the stabilization time scale. Conversely, if the forcing is slowly varying in time compared to the stabilization time scale (e.g., a vortex slowly moving through a steady, but spatially variable windfield as in DM), then the adjustment process should have a time scale appropriate to the "apparent variability" of the environment from a reference frame moving with the vortex. Such a scenario is not intended to be all inclusive, since dynamical situations may exist in which the vortex might be barotropically unstable to asymmetric forcing, or in which temporary continuous spectum growth might occur analogous to the temporary baroclinic growth mechanism studied by Farrell (1982).

Symmetric angular windshear outside the radius of maximum winds can be expected to exert a dominant influence on the stability of any barotropic vortex. Variation between TC motion tracks in NDBT and divergent barotropic numerical models (Anthes and Hoke 1975; Kitade 1981) may suggest that the role of the present stabilization mechanism will be quantitatively modified to the extent that divergence is included. In baroclinic model vortices or in a TC, the role of a barotropic stability mechanism in influencing vortex asymmetries will depend on the competing influence of the inertial stability/instability made possible by the introduction of a secondary circulation into the dynamics. Modeling studies of ocean eddies indicate that coupling between vertical modes can also be expected to alter vortex stability and associated motion (McWilliams and Flierl 1979). Significant radial shear in the tangential winds exists to large heights in a mature TC (e.g., Hawkins and Imbembo 1976, Fig. 13; Frank 1977, Fig. 9). Thus, the essential element that enables the barotropic vortex stability mechanism to operate is certainly present in TCs. In addition, the qualitative similarity of TC motion tracks in baroclinic models (Madala and Piascek 1975; Kitade 1980) to barotropic results provides at least circumstantial evidence suggesting that baroclinic vortex stability is a modification to, rather than being fundamentally different from, barotropic vortex stability. Since the magnitude of TC tangential windshear decreases with height above the boundary layer and with increasing radius outside the radius of maximum winds, a barotropic stability mechanism should be most influential in the region where the TCs convective forcing is initiated.

The present model is being extended to investigate steady-state NDBT vortex asymmetric structure and associated motion of the vortex center in response to explicit forcing. The new model will include variable non-Rankine symmetric vortex structure to retain the potential influence of discrete asymmetric normal modes as well as to facilitate further analysis of the dependence of vortex asymmetries and motion on the structure of the symmetric vortex as recently identified by Chan and Williams (1987) and FE. In principle, the analytical method can be extended to a multilayer quasi-geostrophic dynamical system, which may provide some insights into the influence of baroclinity on TC stability and motion.

Acknowledgments. The authors would like to thank Prof. Russell Elsberry, Dr. Greg Holland and Dr. Lee-Or Merkine for many helpful discussions. This research was in part conducted for the Office of Naval Research (Marine Meteorology Program) and was funded by the Naval Postgraduate School. The numerical calculations were carried out at the W. R. Church Computer Center of the Naval Postgraduate School.

REFERENCES

Adem, J., 1956: A series solution for the barotropic vorticity equation and its application in the study of atmospheric vortices. *Tellus*, **8**, 364–372.

Anthes, R. A., and J. E. Hoke, 1975: The effect of horizontal divergence and the latitudinal variation of the Coriolis parameter of the drift of a model hurricane. *Mon. Wea. Rev.*, **9**, 757–763.

Anthes, R. A., 1982: Tropical cyclones: their evolution, structure and effects. *Meteor. Monogr.*, Vol. 19, No. 41, Amer. Meteor. Soc., 208 pp.

Boyd, J. P., 1983: The continuous spectrum of linear Couette flow with the Beta effect. *J. Atmos. Sci.*, **40**, 2304–2308.

Case, K. M., 1960: Stability of plane couette flow. *Phys. Fluids*, **8**, 143–148.

Chan, J. C.-L., 1986: Supertyphoon Abby—An example of present track forecast inadequacies. *Wea. Forecasting*, **1**, 113–126.

——, and W. M. Gray, 1982: Tropical cyclone movement and surrounding flow relationship. *Mon. Wea. Rev.*, **110**, 1354–1374.

——, and R. T. Williams, 1987: Analytical and numerical studies of the Beta-effect in tropical cyclone motion. Part I: Zero mean flow. *J. Atmos. Sci.*, **44**, 1257–1265.

Cheney, R. E., and P. L. Richardson, 1976: Observed decay of a cyclonic Gulf Stream ring. *Deep-Sea Res.*, **23**, 143–155.

DeMaria, M., 1985: Tropical cyclone motion in a nondivergent barotropic model. *Mon. Wea. Rev.*, **113,** 1199–1210.

Farrell, B. F., 1982: The initial growth of disturbances in a baroclinic flow. *J. Atmos. Sci.*, **39,** 1663–1686.

——, 1987: On developing disturbances in shear. *J. Atmos. Sci.*, **44,** 2718–2727.

Fiorino, M., and R. L. Elsberry, 1989: Some aspects of vortex structure related to tropical cyclone motion. *J. Atmos. Sci.*, **46,** 975–990.

Flierl, G. R., V. D. Larichev, J. C. McWilliams and G. M. Reznik, 1980: The dynamics of baroclinic and barotropic solitary eddies. *Dyn. Atmos. Oceans,* **5,** 1–41.

Frank, W. M., 1977: The structure and energetics of the tropical cyclone. I: Storm structure. *Mon. Wea. Rev.*, **105,** 1119–1135.

Hawkins, H. F., and S. M. Imbembo, 1976: The structure of a small, intense hurricane, Inez 1966. *Mon. Wea. Rev.*, **104,** 418–442.

Holland, G. J., 1983: Tropical cyclone motion: Environmental interaction plus a Beta effect. *J. Atmos. Sci.*, **40,** 328–342.

——, 1984: Tropical cyclone motion: A comparison of theory and observation. *J. Atmos. Sci.*, **41,** 68–75.

JTWC Staff, 1987: Tropical cyclones of the Western North Pacific, 1986. *Mar. Wea. Log,* **31,** No. 4, 11–18.

Kao, S. K., 1955: Wave motion in a rotating Couette flow of a viscous fluid. *Tellus,* **7,** 372–380.

Kasahara, A., 1957: The numerical prediction of hurricane movement with the barotropic model. *J. Meteor.*, **14,** 386–402.

Kitade, T., 1980: Numerical experiments of tropical cyclones on a plane with variable Coriolis parameter. *J. Meteor. Soc. Japan* **58,** 471–488.

——, 1981: A numerical study of the vortex motion with barotropic models. *J. Meteor. Soc. Japan,* **59,** 801–807.

Madala, R. V., and S. A. Piacsek, 1975: Numerical simulation of asymmetric hurricanes on a β-plane with vertical shear. *Tellus,* **27,** 453–467.

McCalpin, J. D., 1987: On the adjustment of azimuthally perturbed vortices. *J. Geophys. Res.*, **92,** 8213–8225.

McWilliams, J. C., and G. R. Flierl, 1979: On the evolution of isolated nonlinear vortices. *J. Phys. Oceanogr.*, **9,** 1155–1182.

Merrill, R. T., 1984: A comparison of large and small tropical cyclones. *Mon. Wea. Rev.*, **112,** 1408–1418.

Mied, R. P., and G. J. Lindemann, 1979: The propagation and evolution of cyclonic Gulf Stream rings. *J. Phys. Oceanogr.*, **9,** 1183–1206.

Pedlosky, J., 1964: An initial value problem in the theory of baroclinic instability. *Tellus,* **16,** 12–17.

Willoughby, H. E., 1988: Linear motion of a shallow-water, barotropic vortex. *J. Atmos. Sci.*, **45,** 1906–1928.